Device-free Detection of Approach and Departure Behaviors using Backscatter Communication

Han Ding*, Chen Qian†, Jinsong Han*‡, Ge Wang*, Zhiping Jiang*, Jizhong Zhao*, Wei Xi*,
*Xi'an Jiaotong University
†University of California Santa Cruz
‡Carnegie Mellon University
Email: {dinghanxjtu,wangge.xjtu,jzp.cs,zjz,weixi.cs}@gmail.com
cqian12@ucsc.edu
jinsongh@andrew.cmu.edu

ABSTRACT

Smart environments and security systems require automatic detection of human behaviors including approaching to or departing from an object. Existing human motion detection systems usually require human beings to carry special devices, which limits their applications. In this paper, we present a system called APID to detect arm reaching by analyzing backscatter communication signals from a passive RFID tag on the object. APID does not require human beings to carry any device. The idea is based on the influence of human movements to the vibration of backscattered tag signals. APID is compatible with commodity off-the-shelf devices and the EPCglobal Class-1 Generation-2 protocol. In APID an commercial RFID reader continuously queries tags through emitting RF signals and tags simply respond with their IDs. A USRP monitor passively analyzes the communication signals and reports the approach and departure behaviors. We have implemented the APID system for both single-object and multi-object scenarios in both horizontal and vertical deployment modes. The experimental results show that APID can achieve high detection accuracy.

Categories and Subject Descriptors

C.2.m [[**Computer System Organization**]]: Computer Communications Networks

Keywords

Wireless sensing; RFID

1. INTRODUCTION

Human motion detection enables tremendous convenience for numerous automated computing systems, including smart control and environments, military and civil security systems, and virtual reality. In particular, detecting human approach and departure behaviors is already an essential function for a wide spectrum of applications. For example, approach detection can guide visual impaired people to grasp the desired object, create alarms when a hand is approaching towards dangerous or fragile objects (electric outlet, thermos, *etc.*), or activate a remote pneumatic switch for a senior person in a wheelchair.

Current approach detection schemes mainly rely on technologies that use imagers, biological signals (such as electromyography (EMG), electroencephalography (EEG)), or special sensors (for example, tactile sensors). However, existing solutions are either impractical in some circumstances or extremely expensive. The imager based approach uses cameras to capture a sequence of images or videos containing the user's movements or appearance and then utilizes pattern recognition techniques to identify the human movements [16, 26]. A critical limitation of imager based approaches is that cameras usually demand good lighting conditions or image quality. Moreover, privacy concern also raise barrier for their implementation. Device-based solutions, such as those using the Brain and Machine Interference (BMI) technology [15, 25], are inconvenient and inflexible for users in their daily life. Another recent advance is to embed specific sensors, including magnet sensors, micro-switches, and tactile sensors *etc.*, in physical space to monitor the human gestures or movements [5, 18]. These approaches suffer from high deployment cost. In a short summary, above solutions all require specific devices or infrastructures, leading constraints to users or incurring high overhead.

In this paper, we propose a device-free approach detection system based on backscatter communication of Ultra High Frequency (UHF) passive Radio Frequency Identification (RFID) tags, called APID. APID has no constraints to users and can reuse the existing RFID infrastructure, which is widely deployed in many smart environment systems. The basic idea is motivated from the following observation of our preliminary experiments. The approach or departure of a hand towards a tag will cause evident and special variations of its backscatter signals. To collect these signals, we introduce a monitor to APID. In practice, we deploy the monitor over Universal Software Radio Peripheral (USRP) [4] for passively overhearing the communication between the reader and tags. Thus, by analyzing and estimating the signal variations, APID can detect the approach and departure behaviors towards tags.

UbiComp '16, September 12-16, 2016, Heidelberg, Germany

DOI: http://dx.doi.org/10.1145/2971648.2971699

We formally model and analyze the signal changes of the tag when an individual user's hand approaches or departs from it. Then APID calculates the Energy Spectrum Density (ESD) of every tag's signal, and determines the behavior from the trends of ESD variations. We overcame a critical challenge in APID when there are multiple tags coexisting. The monitor needs to correlate the collected signals to their source tags, given that there is no effective and stable way to differentiate tag signals when a human body moves around. To solve this issue, we design a decoder algorithm to accurately separate different tags' data. Then we extract Coefficient of Variation (CV) feature of continuous tag signals to determine the approach target of the user.

We have implemented a prototype of APID using a commercial Impinj RFID reader model R420 and passive tags from two manufactures (*i.e.*, Impinj and Alien). The monitor is implemented by USRP N210 with a SBX daughterboard. In particular, APID operates in the area covered by its monitor's antenna. For example, if we deploy the antenna under a table such that the surface of the table is effectively under surveillance, APID can conduct hand-approach detection to the tagged objects on the whole table. Note a monitor can have multiple antennas to cover different areas simultaneously. We conducted extensive experiments in various scenarios. Fifteen volunteers participate in the experiments. The experimental results show that APID can achieve high estimation accuracy. For example, APID correctly detects the approach and departure behaviors with the accuracy of about 93.3%; and in nearly 92% of our tests, APID can identify the real target of a volunteer with up to ten tags coexisting.

2. RELATED WORK

Prior works related to detecting approach or departure behaviors span a wide spectrum, mainly including the camera based, biological signal based, and wireless signal based schemes.

Camera based schemas: Camera based schema is an important part of movement detection systems. These works often capture a sequence of images or videos through cameras, and build a movement indicator utilizing image processing and pattern recognition techniques [14, 16]. Camera based technique usually requires good lighting conditions of the environment. Other concerns, such as the privacy issue, also raise barrier for its application.

Biological signal based schemas: A wide corpus of research has concentrated on using specific equipment, such as the electromyography (EMG) [10, 27] or electroencephalography (EEG) electrodes [12, 15], to estimate human behaviors or movements. Zhao *et al.* [27] collect data about the EMG signals related with the given basic actions, and establish the correlation between them using classifiers or BP neural network technique. In addition, Lew *et al.* [15] detect self-paced upper limb movements from scalp electroencephalograph (EEG) signals. The key limitation of biological signal based works is that they require attaching to or even embedding sensing devices into the human body, which is extremely inconvenient in daily life.

Wireless signal based schemas: Some works [1, 2, 7, 11, 20, 21] have shown the feasibility of using wireless signals (such as WiFi, Z-wave, 60G radios) for motion or activity detection. Sigg *et al.* [22] propose to utilize RSS values of WiFi signals to recognize four activities, including walking, lying, crawling, and standing. They achieved an accuracy (>80%) in the activity recognition, and prove that RSS values can be used for recognizing these macro-movements. However, their work is not suitable to recognize the micro-movements such as moving hands [3] or fine-grained approach detection in a short range. WiTrack [1] tracks the 3D motion of a user using specially designed radar signals, *i.e.*, Frequency Modulated Carrier Wave (FMCW) signals. RF-IDraw [24] attaches a UHF passive tag to the human's finger and leverages two readers and eight omni-directional antennas to track the tag trajectory, and hence infer human's writings. These techniques are either device-based, or requiring specially designed devices and complicated signal processing techniques before conducting the movement detection, limiting their application scope in practice. Compared to prior works, APID adopts new signal processing methods and schemes that are suitable for the Commercial-off-the-shelf (COTS) RFID (only several cents) transmission. It is fully compatible with the commercial RFID standard and can reuse RFID frastructures which may have already been deployed in many environments for object tracking purpose.

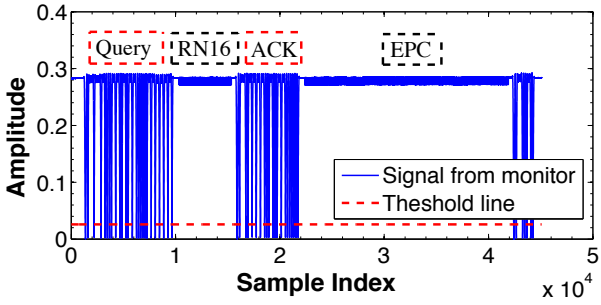

Figure 1: EPCglobal C1G2 backscatter protocol. Signals from both endpoints are collected in our experiment.

3. BACKSCATTER COMMUNICATION IN RFID SYSTEMS

In this section, we introduce the backscatter communication protocol of UHF passive RFID systems. We then take an overview of APID.

Communication in passive RFID systems is based on backscatter radio links. Passive tags carry no battery or radio transmitter. Instead, they harvest power from the reader. The EPCglobal Class-1 Generation-2 (*i.e.*, ISO 18000-6C) protocol is the mainstream industrial standard detailing the interaction between a UHF RFID reader and passive tags. EPCglobal C1G2 is a reader-talks-first protocol [9]. The reader chooses the communication parameters and controls the process based on a slotted ALOHA mechanism. The reader queries tags in its read zone. Each tag randomly selects a slot to reply with a 16-bit random number, *i.e.*, the `RN16`. If the reader receives only one tag response and can decode the number, it sends an `ACK` to acknowledge the tag. Then the tag replies with its Electronic Product Code (`EPC`), *e.g.*, ID. Fig. 1 shows the signals from both endpoints during the procedure captured by our monitor, which clearly illustrates the standard communication process.

3.1 Modulation and Data Encoding

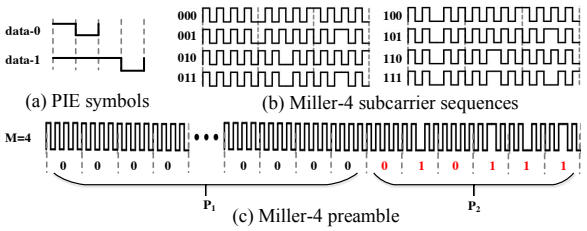

Figure 2: RFID modulation and data encoding schemes.

In this subsection, we briefly introduce the modulation and data encoding methods of EPCglobal C1G2.

3.1.1 Reader-to-Tag communication

Due to the limited computing capability of passive tags, an RFID reader uses Amplitude-Shfit Keying (ASK) modulation. In ASK, digital bits are represented as variations in the amplitude of a carrier wave. The reader uses Pulse Interval Encoding (PIE) to encode data. As shown in Fig. 2(a), a high value and a same-length low value combine to represent a bit '0'. The combination of a longer high value and a short low value represents a bit '1'. In addition, high values correspond to transmitted continuous wave (CW), whereas low values represent attenuated CW. Since the reader supplies energy for passive tags through these high values, PIE encoding is suitable for tag's power-harvesting property. The design of proposed tag EPC extraction algorithm is based on this characteristic of PIE.

3.1.2 Tag-to-Reader communication

The encoding scheme for the tag-to-reader link is determined by the reader. Optional schemes include FM0 (*i.e.*, bi-phase space) and Miller-modulated subcarriers (Miller-2, Miller-4, Miller-8). The Miller schemes are binary-phase-shift-keyed. It provides better interference rejection than FM0. A higher-value Miller method corresponds to slower data transmission. In our system, we config the coding scheme as Miller-4 for a good balance. Miller-4 means that four cycles of the subcarrier are needed for encoding each bit. As shown in Fig. 2(b), a bit '1' of Miller-4 contains a state transition in the middle of its four symbols, while a bit '0' does not, which is the basis of our proposed decoder algorithm proposed.

3.2 System Overview

APID consists of three main components, a commercial RFID reader (Impinj Reader R420), a number of objects (each of them attached with a tag), and a monitor (a USRP N210 with a SBX daughterboard). The reader queries tags by transmitting commands and CWs. The role of the monitor is to passively monitor the communication between the commercial off-the-shelf reader and tags, analyzing the backscattered signals from tags, and differentiating the human hand behaviors. In the prototype APID, we implement the monitor using a USRP model N210, which offers a solution for prototyping RF applications and supports physical layer signal processing [17].

APID works in two scenarios. **1) Single-object scenario.** When a human hand is moving towards or departing from an object attached with a tag, APID should detect this movement. **2) Multi-object scenario.** When the human hand is moving towards an object among multiple objects, APID is able to recognize which object s/he intends to touch.

4. MODEL AND INSIGHT

In this section, we develop a theoretical model of the impact of human approach behaviors to backscatter signals, which will then be utilized by APID for approach detection.

Due to the multipath effect, in real environments the RF wave emitted from a reader to query a tag usually interacts with many other objects around the tag. Hence the integrated waves consist of the ones along direct path between the reader and tag, and those that are *reflected*. For backscatter communication, the most important and ubiquitous reflectors are the floors and walls. In many buildings, floors and walls are constructed by concrete, which has a refractive index around 2.5 and can act as an effective reflector [8]. Let us consider a stable RFID system, the integrated signal received by the tag can be formulated as:

$$S\cos(wt) = s_d\cos(wt) + s_f\cos(wt+\theta_f) + s_w\cos(wt+\theta_w) \quad (1)$$

where s_d, s_f, and s_w represent the signal of direct path, the signal reflected by floors and walls respectively. θ_f and θ_w are the phase differences between the reflected waves and the wave along the direct path. The values of θ depend on the relative length of the path that each wave travels. Since the ambient factors are stable, we can conclude that $S\cos(wt)$ will remain nearly time invariant with no human interference. For simplicity, we rewrite Equation 1 as:

$$S\cos(wt) = s_c\cos(wt+\theta_c) \quad (2)$$

Similarly, when there is a part of human body (*i.e.*, the hand) moving towards the tag, another reflected wave will be introduced. In this case, we can describe the newly integrated signal by the following equation:

$$S^{'}\cos(wt) = \underbrace{s_c\cos(wt+\theta_c)}_{constant} + \underbrace{s_h\cos(wt+\theta_h)}_{variation} \quad (3)$$

where s_h denotes the signal induced by the hand. As indicated by Equation 3, the new signal is composed of two parts, the constant part and the variation part. It indicates that the reflected signal caused by the hand is of counter-intuitively importance. When the hand is moving, the traveling path of RF signals between the constant part and the hand-reflected part changes. In theory, a change of 8cm (a quarter of the wavelength) along that path produces a 90° phase shift, resulting in a change of the signal from a maximum value (or minimum value) to zero. This means that continuous integrated signals will repeatedly oscillate as the hand is approaching the tag or moving away from it.

We further consider the amplitude of the oscillation. As illustrated in Fig. 3, the reader antenna is mounted on the ceiling, tracking the tags within its reading region. A hand is getting closer to a tagged cup. We model the signal transmission path as a triangle, where A represents the antenna, T represents the tag, and H_i represents the moving hand. Let L_i denotes the path length of $A \rightarrow H_i \rightarrow T$. When H is approaching T, we can derive that:

$$\begin{cases} L_j < L_i \\ 0 \le i < j \le n \end{cases} \quad (4)$$

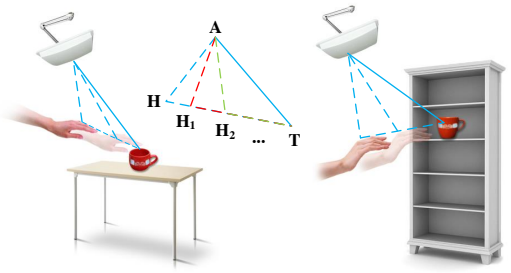

Figure 3: The model of RF signal transmission with approaching behaviors. The monitor is hidden under the table or behind the shelf.

It is known that a shorter path incurs lower attenuation to the signal, resulting in larger amplitude. Thus, according to Equation 4, we can infer that when H is getting closer to T, the amplitude of the oscillation will become larger. Conversely, the amplitude will decrease when H is moving away from T.

Thus, we have the following insight about the change on RF signals corresponding to the hand movement.

Insight: *The continuous RF signals oscillate with the hand movement and can be utilized to differentiate approaching from departure based on the variation tendency of the oscillation.*

5. IDENTIFYING APPROACH AND DEPARTURE BEHAVIORS

In this section, we present the method to analyze backscatter signal variations in practical RFID systems and validate the theoretical results.

5.1 System Setup

We set up the experiment scenario as shown in Fig. 12. Like most RFID applications, the reader antenna is mounted on the ceiling in APID. We invite a volunteer to slowly move his hand to the tagged cup and then move away from it. This test is repeated several times. Our initial attempt was to collect the radio signal strength (RSS) and phase values from the commodity off-the-shelf (COTS) reader during the test. Unfortunately, the results did not show any regular patterns. We conjecture the reasons as follows. First, the granularity or resolution of RSS values reported by the commercial reader is not high. RSS values have been proved effective for identifying some macro-movements, including walking, lying, crawling, and the like [22]. However, since RSS values only provide coarse-grained information about the channel variations. They are not suitable to recognize micro-movements in the device-free scenario [3], resulting in discontinuous or insignificant RSS fluctuations with hand movements. Second, the phase is a periodic function of 2π, and its value highly depends on the location of the tag, which cannot well reflect the approach or departure behaviors. The failure of the above attempt implies that the COTS reader cannot afford the distinction on the approach behavior towards a specific target. Thus, we design a monitor, which sits near the tagged object and passively listens to, records, and analyzes the RF communication between the COTS reader and tags.

Com.	Descriptor	Bit
Query	1000	22
QueryRep	00	4
QueryAdjust	1001	9
ACK	01	18

Table 1: Reader Commands and Parameters

5.2 Signal Preprocessing

In UHF passive RFID systems, a commercial reader can query a tag and receive its replies for hundreds of times per second. The monitor device can record the signals of each complete inventory on a specific tag, as shown in Fig. 1. To verify the aforementioned theoretical analysis and further identify gestures, we need to extract the backscatter signals from the collected mixed signals.

In a common backscatter communication process, two types of messages are sent by a tag, *i.e.*, RN16 and EPC. We choose to use the EPC signals as the source for subsequent analysis. EPC is the unique identifier of a tag, and we can extract the tag's ID from the EPC message. We develop the `EPC Filter` module in the monitor. It allows the monitor to accurately retrieve the EPC message from communication signals. The EPC filter has two procedures: coarse-grained segmentation and fine-grained localization.

5.2.1 Coarse-grained Segmentation

Coarse-grained segmentation module aims to differentiate between reader commands and tag replies. After this module, we can derive the coarse EPC sequence. The strategy is detailed in the following.

According to the EPCglobal C1G2 protocol, tag replies EPC after receiving an ACK command from the reader. Based on this fact, we can derive the coarse-grained EPC segment between the ACK and a subsequent reader command. The reason why we utilize reader commands to seek for EPC is that: the reader's signal has higher SNR and larger amplitude, which makes it easier to be located and decoded. Table 1 shows the reader's commands and their parameters specified by the protocol. We can see that every command has its unique descriptor. It inspires us to locate an ACK easily by decoding its descriptor. As Fig. 4 shows, starting with a frame-sync (composed of a fixed-length start delimiter, a data-0, and an R⇒T calibration (RTcal)), ACK has two parts: a 2-bit descriptor and a 16-bit RN16. We can choose a low threshold (Fig. 1) to locate reader commands and then decode a command by comparing every pulse width with Table 2. These parameters are the basic components of every reader command, and the lengths of them are specified by the protocol, among which *Tari* is in the range of 6.25μs to 25μs, and the choice of Tari shall in accordance with local radio regulations (Tari = 25μs in our implementation). For better fault-tolerance, we extends the length by $\pm$20%.

5.2.2 Fine-grained Localization

We get the coarse-grained EPC segment between the end of ACK and the begin of the next command; nevertheless, this EPC segment includes many carrier samples, such as the first 500 samples shown in Fig. 6(a). Falsely including these

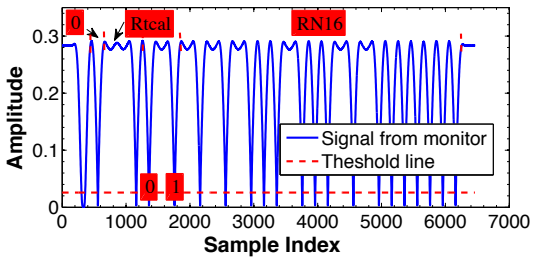

Figure 4: ACK command under PIE encoding collected by the monitor.

Com.	Time duration	Length	Range
RTcal	[2.5Tari,3.5Tari]	600	480∼720
TRcal	[1.1RTcal,3.0RTcal]	700	560∼864
Data-0	1 Trai	220	176∼264
Data-1	[1.5Tari,2.0Tari]	360	288∼432

Table 2: Reader Command Components and Parameters

samples may affect the subsequent signal energy estimation. Therefore, we need to further find the start point of the EPC segment from the raw signal samples. We term this process as fine-grained EPC localization.

In our experiments, we observe that the signals of different tags may locate in different positions. Sometimes a tag signal is higher than the carrier but in some other cases it is lower than the carrier. As a result, we cannot determine a certain threshold to find the start point. To solve this problem, we apply the *Absolute Forward Difference* (AFD) method to accurately localize the start point of EPC.

Given an EPC sequence $E = (e_1, e_2, ..., e_K)$, the AFD value is calculated by:

$$\triangle E = |e_{k+1} - e_k|, k = 1, 2, ..., K-1. \quad (5)$$

The AFD result of the EPC signal in Fig. 6(a) is shown in Fig. 6(b). Utilizing the obvious amplitude difference of carrier signals and real EPC signals, we can now employ a simple threshold method to quickly find the first sample of E, as the red circle outlined in the two subfigures. In fact, AFD is with good compatibility and resilient to the impact from the tag heterogeneity and environmental factors.

5.3 Identifying Approach and Departure Behaviors

In this subsection, we verify the theoretical results aforementioned and utilize the EPC variation trend to identify approach and departure behaviors.

EPC is encoded in a pulse-like way, implying the energy in the signal. The energy of a signal $x(t)$ is usually represented as:

$$\int_{-\infty}^{\infty} |x(t)|^2 dt \quad (6)$$

In our implementation, we use *Energy Spectrum Density* (ESD) [19] to characterize the energy. ESD can tell how the energy of a signal is distributed with frequency. Pulse-like signals usually have finite amount of energy. *Parseval's Theory* [23] provides another expression of the energy of a signal in terms of its Fourier transform, that is,

$$\hat{x}(f) = \int_{-\infty}^{\infty} e^{-2\pi i f t} x(t) dt \quad (7)$$

Thus, we have the following equation,

$$\int_{-\infty}^{\infty} |x(t)|^2 dt = \int_{-\infty}^{\infty} |\hat{x}(f)|^2 df \quad (8)$$

Here f is the frequency measured in Hz. ESD is so called because the integrand $|\hat{x}(f)|^2$ can be regarded as a density function, which describes the energy per frequency unit of the signal. In this case, we estimate the ESD of a signal $x(t)$ as [23]:

$$S_{xx}(f) = |\hat{x}(f)|^2 \quad (9)$$

To evaluate the effectiveness of our method, we invite a volunteer to participate in our experiments. He moves his hand approaching to the tagged cup, then moves away from it. The monitor records the signals during the procedure. The data independence should be guaranteed when conducting signal analysis. To this end, we adopt the P_1 part of the EPC preamble as the source signal in this module since the waveform of this part is constant for various tags (refer to Fig. 2). The first 50 points of one P_1's ESD values are shown inFig. 5(a). We find that most of the ESD values are concentrated in its first 10 points. Therefore we choose to include the first 10 values into consideration in APID. We normalize their values and consider the mean as the ESD of one EPC. Fig. 5 (b) and (c) show ESD variations of approach and departure behaviors, respectively. We observe that they validate our insight from the theoretical model. Human hand movements incur energy oscillations to the replies (*e.g.*, EPCs) of tags, and the movement direction (approach or departure) can be deduced from the vibration increase or decrease. Inspired by this observation, to distinguish the two gestures, we adopt *Dynamic Time Warping* (DTW) technique to compute the similarity between an unknown movement and the template of approach or departure movement. The benefit is that DTW can automatically compress or stretch a sequence to focus on the shape similarity of two sequences. This can handle the problem of the disagreement on duration or amplitude of different users' movements. Detailed description of this algorithm is skipped due to space limit. In addition, we also investigate the ambient interference for comparison. We show the ESD variations when a person walks 20cm, 1m, and 1.5m away from the tag in Fig. 5(d). The results suggest that the incurred noise can be easily filtered by the preprocessing (*i.e.*, comparing the DTW distance with a predefined threshold), since the signal variation tendency is irregular and inconsistent with either the approach or departure behavior.

6. MULTI-OBJECT SCENARIOS

In the previous section, we solve the problem of identifying whether a user is approaching an object in a single-object scenario. However, in real circumstances, like a table or a shelf, there could be more than one object, each of which carries a passive tag. In this section, we present the solution to find the true approach target of the human hand in multi-object scenarios.

6.1 Challenges

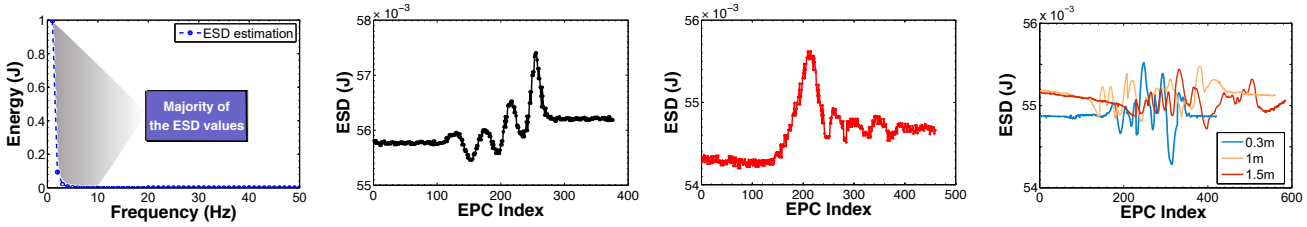

(a) ESD (b) Approach behavior (c) Departure behavior (d) Walking

Figure 5: (a) Energy of an EPC under different frequencies. For a clearer illustration, we only show the first 50 points among the total 940 points. (b) ESD sequences of an approach behavior. (c) ESD sequences of a departure behavior. (d) ESD sequences when a person walks near the tag.

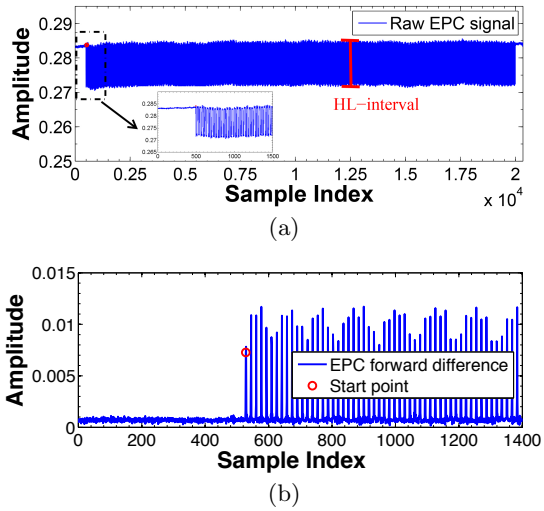

(a)

(b)

Figure 6: Fine-grained EPC localization. (a) The raw EPC segment. (b) The AFD of the raw EPC samples.

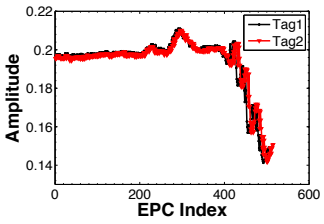

Figure 7: Amplitude changes of two tags when a hand is approaching one of them.

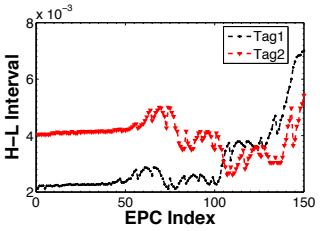

Figure 8: H-L interval changes of two tags when a hand is approaching one of them.

According to the specifications in EPCglobal C1G2, multiple tags can reply their EPCs to the reader in random orders in one inventory round using the slotted ALOHA protocol. The monitor can capture EPC messages but it cannot decode those messages, *i.e.*, extracting the IDs of these tags like a COTS reader to distinguish them. Therefore, APID needs to resolve two main problems. First, it should differentiate tag signals based on their sources. Second, it should find the tag whose signal has the most prominent change, which indicates the target of an approach behavior.

To begin with, we attempt to pursue proper features in the signal level to solve the first problem. We put two tags on a table with a 30cm distance in between. Then a volunteer moves his hand to one of them. We try mainstream features used by prior works in fingerprinting wireless signals, including Entropy, Power Spectral Density (PSD), Pulse Amplitude, Mean Square Error (MSE), Mean, and Variance, *etc.*. Unfortunately, during the movement of user's hand, the tag signal varies with time, and we could not find appropriate features which can uniquely and stably represent a specific tag. We present the attempt of using two representative features as following.

Amplitude. Fig. 7 plots the amplitude of these two tags' EPC signals. We see that they almost overlap with each other. The reason behind may be that tags' signals are all modulated based on the reader transmitted carrier waves, so all tag signals shall change consistently as the carrier.

HL-interval. In addition, due to the hardware heterogeneity [6], when modulating a same logic data '0' or '1', tags yield different intervals between the high level and low level values. We denote such an interval as a HL-interval. We plot an example of HL-interval in Fig. 6(a). As shown in Fig. 8, the HL-interval of a tag is distinct and stable for the first 50 points. It seems that HL-interval is a good choice for differentiating tags. What disappoints us is that when the hand is moving (starting from the time of near 50th point), both tags' signals are influenced. Their HL-interval values cross with each other at about 110th point and become indistinguishable.

In summary, an approach behavior has complex impact on the tag signal, and it is difficult to find a unique feature to distinguish signals from different tags.

6.2 Differentiating tag signals

In this subsection we solve the first problem: differentiating signals from different tags. Leveraging the architecture of EPC memory and characteristics of Miller-4 encoding (refer to Section 3.1.2), we implement an `EPC decoder` module, which includes a `recoder` algorithm and a `decoder` algorithm.

It is worth to briefly introduce the composition of the EPC memory. As the ID or identifier of each tag, the EPC memory contains PC, EPC and CRC-16, which are stored in the order of the most significant bit first (MSB). In particular, PC is 16-bit long, and its first 5 bits (denoted as $\texttt{PC}_5$) define the EPC length. For example, $PC_5 = 00110$ means the EPC

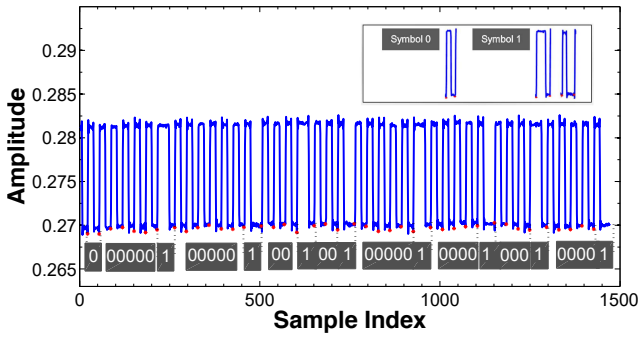

Figure 9: An example of the recoder.

is 6-word long. In addition, the maximum length of EPC is 6 words (*e.g.*, 96 bits) specified by EPCglobal C1G2. For simplicity, we use a part of the EPC signal collected from a 96-bits long tag to illustrate the following algorithms.

6.2.1 *Recoder*

For passive RFID systems when tag EPC is encoded in Miller-4, it means that a bit contains 4 subcarrier cycles, as illustrated in Fig. 2. Under a 10M/s sampling rate, the number of samples of a subcarrier cycle is constant, *i.e.*, about 30 in total, while 15 are for high level values, other 15 are for low levels. We recode such a subcarrier cycle (with same length of high level and low level) as symbol '0'. Our recoder detects the last point of the low state for every subcarrier, as the red points shown in Fig. 9. Hence, the recoded symbols '0' and '1' can be differentiated by comparing the interval (ΔI) of adjacent red points. If $\Delta I > M$, we get a symbol '1' ($M = 40$ in our implementation). Otherwise, we get a symbol '0'. Fig. 9 illustrates a part of Miller-4 encoded EPC, composed by P_2 of preamble (*e.g.*, 010111, refer to Fig. 2(c)) and PC_5 (*e.g.*, 00110). The recoded sequence is marked in grey boxes, which is the input of the following decoder algorithm.

Algorithm 1: EPC Decoder

Input: Symbol sequence: $S = (s_1, s_2, ...s_n)$
Initial $b : K$
The number of bits need to be decoded: L
Output: Bit sequence: $B = (b_1, b_2, ..., b_L)$

```
1: i ← 0, b ← K, e ← K + 3
2: while i < L do
3:    t ← S(b : e)
4:    if t(2) == 1 then
5:       B(i) = 1, b ← e + 1, e ← b + 3
6:    else if t(3) == 1 then
7:       B(i) = 1, b ← e, e ← b + 3
8:    else
9:       B(i) = 0
10:      if t(1) == 1 then
11:         b ← e + 1, e ← b + 3
12:      else
13:         b ← e, e ← b + 3
14:      end if
15:   end if
16:   i ← i + 1
17: end while
```

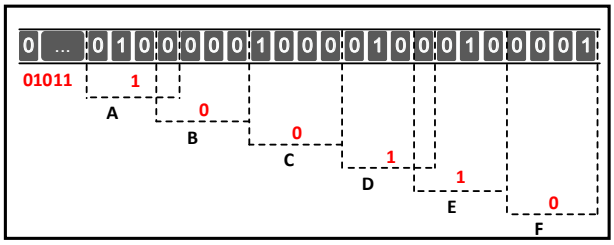

Figure 10: Illustration of the EPC decoder algorithm.

6.2.2 *Decoder*

The decoder algorithm is designed by leveraging the characteristics of Miller-4 encoding. That is, every four subcarrier cycles construct one bit, and bit 1 has an state transition in the middle. We translate every continuous 4 symbols into one bit, and determine the value of the bit by checking the position of the symbol '1'. If symbol '1' locates in the middle of 4 symbols (the 2nd or 3st position), we translate such 4 symbols as a bit 1. Otherwise, we get a bit 0. Moreover, the begin index and end index of the current 4 symbols are determined by the former 4 symbols. The detail of the decoder algorithm is elaborated in Algorithm 1, in which b and e denote the begin index and end index respectively.

As an example, we execute the algorithm on the symbol sequence in Fig. 9. In this example, the input S = '0000001000001001001000001000001000100001', $L = 11$, $K = 1$. The dotted boxes in Fig. 10 illustrate the procedure of our algorithm. For example, we get a bit 1 from the 4 symbols '0100' in box A. Based on the position of symbol '1' (*i.e.*, 3st position), we get the next 4 symbols '0000' and the translated bit 0, as shown in box B. Ultimately, the output bit sequence B = 01011100110, implying that P_2 = 010111 and PC_5 = 00110. This well matches the corresponding part in the real EPC. The result proves that our decoder is able to distinguish different EPCs effectively. Note that above methods can be easily extended to other encode/decode mechanisms adopted by existing COTS passive RFID systems, such as Miller-2 and Miller-8, *etc.*.

6.3 Identifying the Approach Target

Using the unique EPC code, we can separate signals of different tags. We then aim at figuring out the true target of the approach behavior among multiple objects. In APID, our objective is to extract a feature from the replied EPC signals, which can well profile the most prominent influence corresponding to a human hand movement.

In real implementation, tags are different in their H-L intervals. We observe that the signal variation of a tag with high H-L interval is almost always more obvious than that of a tag with low H-L interval. This may cause false alarms when identifying the real target if the user is approaching to the tag with low H-L interval. We show the ESD trends of two tags in Fig. 11 (a) and (b). From the results we see that no matter the volunteer approaches to Tag1 or Tag2, Tag1 (with higher HL-interval) always has larger ESD variation. To address this problem, we propose to utilize the metric of *coefficient of variation* (CV).

We calculate the *coefficient of variation* (CV) of P_1 (guaranteeing the data independence) to reflect the influence. CV

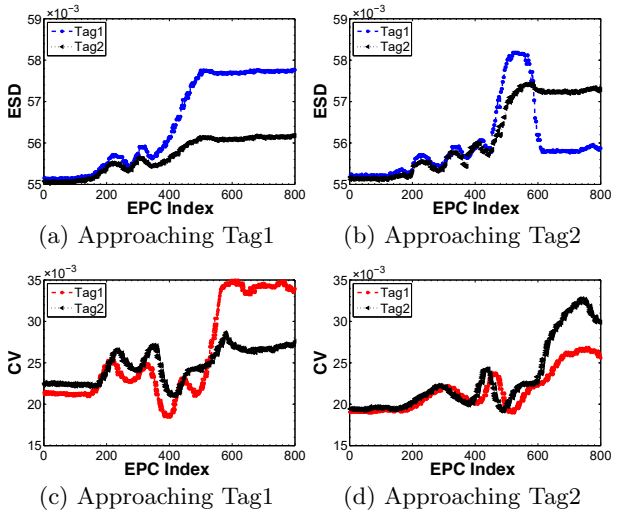

Figure 11: ESD and CV variations of EPC sequences.

is a standardized measure on the dispersion of a probability distribution, defined as:

$$CV = \sigma/\mu \tag{10}$$

where σ is the standard deviation and μ is the mean. It shows the extent of variability in relation to the mean. CV is a dimensionless number, and the actual value of CV is independent of the unit of the measurement. Hence it is suitable for comparison among the data with different means and H-L intervals.

In APID, we can treat the samples of P_1 as a random source, and calculate CV for every P_1 of continuous tag signals. To evaluate the effectiveness of CV, we conduct a group of experiments. We put two tagged objects on the table (among which Tag1 has higher HL-interval), and ask the volunteer to move his/her hand to them, one at a time. Fig. 11 (c) and (d) show the results. When the hand approaches Tag1, its CV variation is larger than that of Tag2. On the contrary, when the hand approaches Tag2, the variation change is opposite. Thus, we propose to regard the tag which has the maximum CV variation as the target that the user actually moves his/her hand to.

7. IMPLEMENTATION AND EVALUATION

In this section, we present the implementation and evaluation of APID.

7.1 Experimental Setup

We build APID using a COTS Impinj Reader R420, 20 passive tags of four tag models from two manufacturers (*i.e.*, Alien 9640, Alien 9662, Impinj E41B, and Impinj H47, each of them costs 5-10 cents). We use a USRP N210 with a SBX daughter board as the monitor [4] to record the physical layer signals transmitting between the reader and tags. The antennas (model Laird A9028R30NF) used by the reader and monitor are both directional. The size of antenna is 25.4cm × 25.4cm × 3.8cm and with 8dBi gain.

The reader antenna is mounted on the ceiling, about 3m apart to the tags. We attach tags to various objects, such as bottles, books, cartons, *etc.*, to verify the effectiveness of APID across different types of dielectric material. Tagged objects are placed following two common display modes, horizontal mode (*i.e.*, simulating a table) and vertical mode (*i.e.*, simulating a shelf). The monitor antenna is deployed under the table or on the back of the shelf. The principle of positioning the monitor is to make sure that the monitor can receive the RF signals backscattered from the tags, while the line-of-sight transmissions between the monitor's antenna and tags are not always blocked. To meet above requirements, it is better that the monitor antenna is closer to tags (say within 50cm).

7.2 Accuracy of Single Tag Scenario

We evaluate APID's accuracy of recognizing approach and departure gestures under different conditions.

7.2.1 *Distance between the hand and the tag*

We first study the effect of distances between the hand and the tag on the detection accuracy. Fifteen volunteers participate in this experiment. Each volunteer performs the approach and departure behaviors for 30 times in each distance, without blocking the tag. Note that the distance here represents the nearest distance during the hand movement, and the volunteer moves at least one arm long. We identify the behavior through the trend of continuous EPC ESD values. The results are shown in Fig. 13. The bar in this figure shows the probability that the ESD trend follows our deduction, *i.e.*, APID correctly determines the gesture. The 'Other' bar expresses the percentage of gestures which cannot be identified by APID based on the ESD trends. The results show that when the distance increases, the detection accuracy decreases. When the distance enlarges to 60cm, more than half of the gestures become unidentifiable. The reason is that when the hand moves farther away from the tag, the influence of the hand reflection to tag signals becomes smaller, resulting in more inapparent oscillations. On the other hand, the detection accuracy remains high when the distance is smaller than 20cm. It means that the data collected when the hand is 20cm away from the object is enough for APID to differentiate the gestures. In common cases, such a distance is reasonable for arm-reachable applications.

7.2.2 *Tag diversity*

Then we evaluate if APID is compatible with different kinds of tags. We invite volunteers to participate in 500 experiments using four kinds of passive tags from two manufacturers. This group of experiments are conducted in horizontal mode. During each experiment, a volunteer was asked to move his/her hand towards a specific tag, or away from it. The result is shown in Fig. 14. It indicates that our approach detection method is applicable for different kinds of tags. And the detection accuracy of Alien tags is higher than that of Impinj tags, which exceeds 96% for both approach and departure behaviors. The reason is the tag model may have certain impact on the backscattered signal as well as the detection performance, due to the different antenna and IC designs. Based on above experiment results, we recommend to use Alien tags for real system deployment and conduct following experiments based on this type of tags.

7.2.3 *Human diversity*

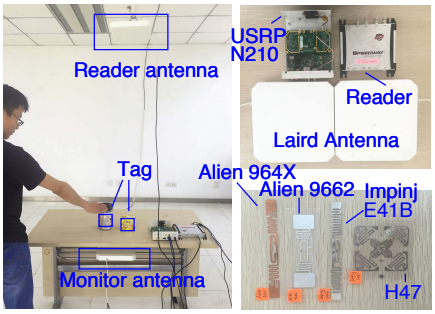

Figure 12: System prototype.

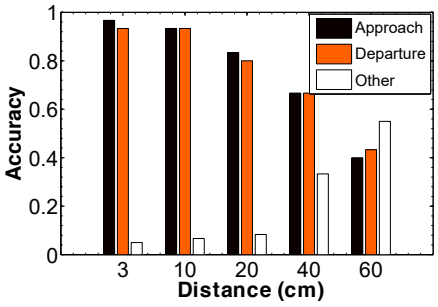

Figure 13: Accuracy *vs* hand-to-tag distances.

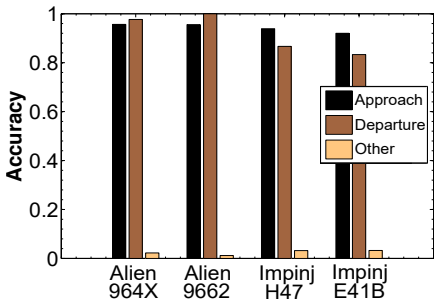

Figure 14: Accuracy *vs* different tags.

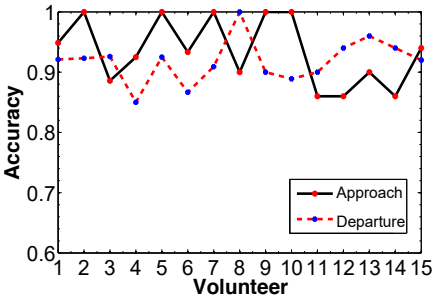

Figure 15: Accuracy *vs* different volunteers.

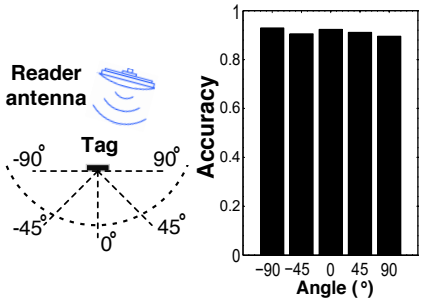

Figure 16: Accuracy *vs* approaching angles.

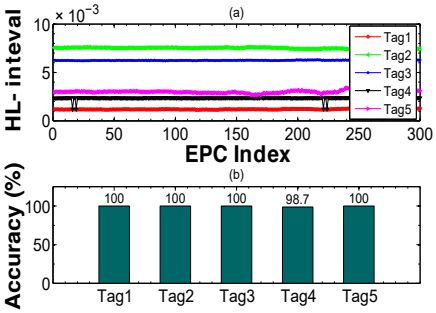

Figure 17: (a) HL-intervals of different tags labeled by the results of our EPC decoder. (b) Accuracy of the decoder.

In this part, we investigate the effect of human diversity on the detection accuracy. We invite fifteen volunteers (age 23 - 30) to conduct this experiment, 50 times for each. Their heights vary from 160cm to 180cm. The result is shown in Fig. 15. The overall accuracy for the fifteen volunteers maintains in a high level, say, 94.3%. Specifically, the minimum accuracy can still reach 85% for volunteer 4's departure behaviors. This indicates that APID works well across different users.

7.2.4 *Approaching angle*

This group of experiments is to investigate the impact of the hand approaching from different angles. We test 5 typical angles, *i.e.*, -90°, -45°, 0°, 45°, and 90° from the line-of-sight between the reader and tag respectively, under the same experimental setups as shown in Fig. 12. Fig. 16 shows the average accuracy of 30 approach motions at each angle. We find that APID shows consistent accuracy for different angles, and the median accuracy is above 90%. The results reveal that varying the direction that a human hand approaches to the tagged object has little affection to the detection accuracy.

7.2.5 *Display mode*

We also examine the performance of detection under two display modes, horizontal and vertical mode. We find that APID performs well in both modes and the accuracy is 94.3% and 92.2% respectively. The results demonstrate that APID can achieve a high estimation accuracy in average, *i.e.*, 93.3%.

7.3 Accuracy of Multi-object Scenario

We then exam the detection accuracy of APID in multi-object scenario. Experiments in this section focus on answering three questions. First, when multiple tags exist in the picking area, can APID successfully differentiate their signals? Second, when the distance between objects changes, can APID still yield good performance? Third, with multiple objects displaying in different modes, how effective is APID?

7.3.1 *Accuracy of EPC Decoding*

To detect the real approach target of the user, the first step is to correctly separate EPC signals of different tags. In this part, we evaluate the effectiveness of our EPC decoder module. As mentioned in Section 6.1, when there is no variation around the tags, the HL-interval of each tag is stable and distinguishable. Thus, we collect signals from 5 Alien tags in a stable environment and distinguish them using their HL-intervals. We treat the labels deduced by HL-invervals as the ground truth, and compare them with the output of our decoder. We plot 300 results of HL-intervals for each tag in Fig. 17(a), the values in different colors are labeled by the results derived from our decoder. From the results, we can obviously determine that there are only 4 errors (for Tag 4) among the overall 1500 tests. The accuracy of our EPC decoder is 98.7%+, as shown in Fig. 17(b).

7.3.2 *Accuracy vs Distance*

It is known that when the tags are closer, the influence from an approach gesture to them is more similar. Thus, we

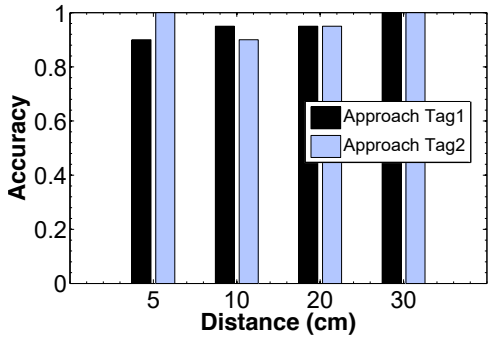

Figure 18: Approach target detection accuracy in multi-object scenario with different distances between tags.

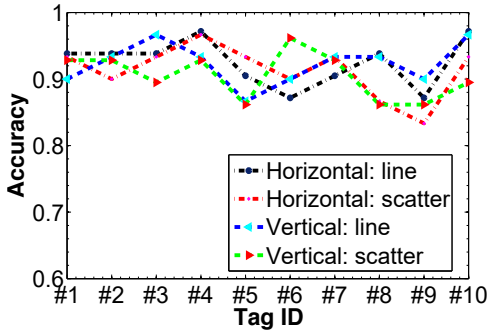

Figure 19: Approach target detection accuracy in multi-object scenario under four deploy modes.

investigate the impact of the distance between tags on the detection accuracy. We put two tagged objects on the table, and invite the volunteers to approach them respectively, 30 times for each. Fig. 18 shows the accuracy with varying tag-to-tag distance from 5cm to 30cm. We observe that at the distance of 5cm, the minimum accuracy, *i.e.*, 90%, is achieved when the hand approaches Tag 1. If enlarging the distance, the detection accuracy increases gradually and reaches 100% at 30cm. In practice, we believe 5cm is a reasonable short distance between tags attached on objects. In this case, APID can still achieve 90% accuracy (3 errors among 30 trials). Thus, if the distance between tags is no less than 5cm, its impact to the APID's detection accuracy will be slight.

7.3.3 *Accuracy vs Multiple tags*

Under each deploy modes, we conduct two types of experiments to verify the approach target detection accuracy among multiple tags. We deploy ten tags in a line with 10cm in between or scatter them at random locations while the minimum distance between any two tags is 5cm. The 15 volunteers are invited to approach to each tagged object 30 times, and we test if APID can correctly verify the target tag. The detection results are shown in Fig. 19. We can see that the accuracy of most detections are above 90%. The maximum number of errors occurs when the volunteer moves his hand to Tag #9 under horizontal mode with tags scattering at the table. In this case, APID considers it approaching to the adjacent tag (Tag #8). Overall, the average accuracy is about 91%. Note that potential options of further improving the accuracy include employing multiple minitors, using customized readers or tags with higher communication frequency, and other solutions that can increase the detection resolution. However, those options might be cost-inefficient.

8. DISCUSSION AND LIMITATION

In this section we discuss the limitations and practical deployment issues of APID.

Object material: Current UHF RFID systems are designed to operate around the frequency of 900MHz, with which the tags function well on the surface of most common materials, including wood, glass, paper, etc. However, RF transmission can be significantly affected by certain materials, such as metal and water, either completely reflecting an incident wave or absorbing it. Thus, APID may not work well for those materials.

Hand moving speed: The hand moving speed has little impacts to the detection accuracy of APID. Since a commodity UHF reader, *e.g.*, Impinj R420, is capable to read more than 1000+ tags per second [13]. Such a high rate allows the reader to collect a large number of responses from the tag attached to the object. The sufficient samples extracted from those responses guarantee a fine-grained monitoring on the hand approach or departure movement regardless of the hand moving speed.

Signal analysis API of commercial readers: We implement the prototype of APID over a USRP based monitor for collecting and analyzing the signals backscattered by tags. If the RFID manufactures enable the corresponding signal analysis functions in their commercial readers and APIs, USRP based monitor is not necessary.

Unauthorized access: So far, APID only focuses on the behavior recognition. Thus, it cannot differentiate unauthorized users or behaviors for some specific applications, such as intrusion detection and access control systems. This is out of the scope of this paper, and we will leave it for future study.

9. CONCLUSION

In this paper, we design and implement APID for near-proximity detection for hand approaching, without carrying special devices. APID is developed based on the observations of the influences of human movements to the vibration of backscattered tag signals, from both experiments and theoretical analysis. APID uses the energy changes of backscatter signals as the feature to identify approach and departure behaviors. The experiments show that APID achieves high detection accuracy. Our future works include enlarging the monitoring range, extending the implementation scope, and enabling a fine-grained body motion detection.

10. ACKNOWLEDGEMENTS

This work was supported by National Basic Research Program of China (973 Program) under Grant No.2015CB351705, NSFC Grant No.61190112, 61325013, 61572396, 61402359, China 863 Grant 2013AA014601, and National Science and Technology Major Project of the Ministry of Science and Technology of China JZ-20150910. Chen Qian is supported by UC Santa Cruz Startup Grant and National Science Foundation grant CNS-1464335. We thank the valuable comments from our shepherd Dr. Vassilis Kostakos and anonymous reviewers.

11. REFERENCES

[1] F. Adib, Z. Kabelac, D. Katabi, and R. C. Miller. 3D Tracking via Body Radio Reflections. In *Proceedings of USENIX NSDI*, 2014.

[2] F. Adib and D. Katabi. See Through Walls with WiFi. In *Proceedings of ACM SIGCOMM*, 2013.

[3] K. Ali, A. X. Liu, W. Wang, and M. Shahzad. Keystroke Recognition Using WiFi Signals. In *Proceedings of ACM MobiCom*, 2015.

[4] M. Buettner and D. Wetherall. A Gen 2 RFID Monitor based on the USRP. *ACM SIGCOMM Computer Communication Review*, 40(3):41–47, 2010.

[5] C. Castellini and R. Koiva. Using a High Spatial Resolution Tactile Sensor for Intention Detection. In *Proceedings of IEEE ICORR*, 2013.

[6] B. Danev, D. Zanetti, and S. Capkun. On Physical-Layer Identification of Wireless Devices. *ACM Computing Surveys (CSUR)*, 45, 2012.

[7] H. Ding, L. Shangguan, Z. Yang, J. Han, Z. Zhou, P. Yang, W. Xi, and J. Zhao. FEMO: A Platform for Free-weight Exercise Monitoring with RFIDs. In *Proceedings of ACM SenSys*, 2015.

[8] D. Dobkin. *The RF in RFID: Passive UHF RFID in Practice*. Elsevier Inc, 2008.

[9] EPCglobal. *Specification for RFID Air Interface EPC: Radio-Frequency Identity Protocols Class-1 Generation-2 UHF RFID Protocol for Communications at 860 MHz-960 MHz*, 2008.

[10] K. H. Ha, H. A. Varol, and M. Goldfarb. Volitional Control of a Prosthetic Knee using Surface Electromyography. *IEEE Transactions on Biomedical Engineering*, 58(1):144–151, 2011.

[11] J. Han, H. Ding, C. Qian, D. Ma, W. Xi, Z. Wang, Z. Jiang, and L. Shangguan. CBID: A Customer Behavior Identification System using Passive Tags. In *Proceedings of IEEE ICNP*, 2014.

[12] J. Ibáñez, J. Serrano, M. del Castillo, J. Gallego, and E. Rocon. Online Detector of Movement Intention based on EEG-Application in Tremor Patients. *Biomedical Signal Processing and Control*, 8(6):822–829, 2013.

[13] ImpinJ. *Speedway installation and operations guide, Version 5.6.2*, 2012.

[14] S. Kohler, M. Goldhammer, S. Bauer, K. Doll, U. Brunsmann, and K. Dietmayer. Early Detection of the Pedestrian's Intention to Cross the Street. In *Proceedings of IEEE ITSC*, 2012.

[15] E. Lew, R. Chavarriaga, H. Zhang, M. Seeck, and J. Del Millan. Self-paced Movement Intention Detection from Human Brain Signals: Invasive and Non-invasive EEG. In *Proceedings of IEEE EMBC*, 2012.

[16] T. Luhandjula, E. Monacelli, Y. Hamam, B. J. van Wyk, and Q. Williams. Visual Intention Detection for Wheelchair Motion. *Advances in Visual Computing*, 5876:407–416, 2009.

[17] U. N210. *https://www.ettus.com/product/details/UN210-KIT*.

[18] Y. Nakauchi, K. Noguchi, P. Somwong, T. Matsubara, and A. Namatame. Vivid Room: Human Intention Detection and Activity Support Environment for Ubiquitous Autonomy. In *Proceedings of IEEE IROS*, 2003.

[19] A. V. Oppenheim and G. C. Verghese. *Signals, Systems and Inference*. Prentice Hall, 2010.

[20] Q. Pu, S. Gupta, S. Gollakota, and S. Patel. Whole-home Gesture Recognition using Wireless Signals. In *Proceedings of ACM MobiCom*, 2013.

[21] L. Shangguan, Z. Yang, A. X. Liu, Z. Zhou, and Y. Liu. Relative Localization of RFID Tags using Spatial-Temporal Phase Profiling. In *Proceedings of USENIX NSDI*, 2015.

[22] S. Sigg, M. Scholz, S. Shi, Y. Ji, and M. Beigl. RF-Sensing of Activities from Non-Cooperative Subjects in Device-free Recognition Systems using Ambient and Local Signals. *IEEE Transactions on Mobile Computing*, 13(4):907–920, 2014.

[23] J. Y. Stein. *Digital Signal Processing: A Computer Science Perspective*. Wiley-Interscience, 2000.

[24] J. Wang, D. Vasisht, and D. Katabi. RF-IDraw: Virtual Touch Screen in the Air using RF Signals. In *Proceedings of ACM SIGCOMM*, 2014.

[25] E. Wentink, S. Beijen, H. Hermens, J. Rietman, and P. Veltink. Intention Detection of Gait Initiation using EMG and Kinematic Data. *Gait & posture*, 37(2):223–228, 2013.

[26] L. Zhang, X.-Y. Li, W. Huang, K. Liu, S. Zong, X. Jian, P. Feng, T. Jung, and Y. Liu. It Starts with iGaze: Visual Attention Driven Networking with Smart Glasses. In *Proceedings of ACM MobiCom*, 2014.

[27] H. Zhao and B. Wang. Configuration of the Mckibben Muscles and Action Intention Detection for an Artificial Assistant Suit. *International Journal of Advanced Robotic Systems*, 9(74), 2012.